

## DIRECT NUMERICAL SIMULATION OF TURBULENT FLOW ABOVE RIBLETS UNDER ADVERSE PRESSURE GRADIENT

**Satoshi Ikeda**

Department of Mechanical Engineering  
Osaka University  
2-1 Yamadaoka, Suita, Osaka 565-0871, Japan  
iked@fluid.mech.eng.osaka-u.ac.jp

**Kie Okabayashi**

Department of Mechanical Engineering  
Osaka University  
2-1 Yamadaoka, Suita, Osaka 565-0871, Japan  
okabayashi@mech.eng.osaka-u.ac.jp

**Shintaro Takeuchi**

Department of Mechanical Engineering  
Osaka University  
2-1 Yamadaoka, Suita, Osaka 565-0871, Japan  
shintaro.takeuchi@mech.eng.osaka-u.ac.jp

### ABSTRACT

Spatially-developing boundary layers above smooth and riblet walls are simulated to investigate the drag-reducing performance of the riblet under an adverse-pressure gradient (APG). Open boundary layer without upper wall is reproduced using rescaling/recycling method in order to set the blowing and suction at the upper boundary and simulate APG. All statistics under the zero pressure gradient (ZPG) are obtained quantitatively until unphysical discontinuous pressure fluctuation occurred. The calculated drag reduction by the riblet is in good agreement with the previous experiment. Under the APG, the separation and reattachment points are qualitatively reproduced, although the results suggest the lack of resolution in the wall-normal direction.

### INTRODUCTION

Reduction of skin friction drag will contribute significantly to improvement of aerodynamic performance, because about half of total drag of aircraft at cruising condition is friction drag. Recently, renewed attention is focused on riblet as a realizable flow control device: a new shape forming method of riblet on the aircrafts have been developed for practical use that overcomes long-pending issues (Kurita et al., 2018). As for introduction of riblet to aircrafts, 2% of total air drag is confirmed by Airbus flight test (Szodruich, 1991). Effective spacing of groove of riblets is micron order at cruising condition.

Drag-reducing performances of the various riblets are intensively investigated by experiments (Bechert et al., 1997). However, drag-reducing performance of riblets on aircrafts differs from that measured in an idealized situation in laboratory. One of the differences is the presence of pressure gradient. It is reported that the mild adverse pressure gradient (APG) brings favorable effects on performance of riblets (Viswanath, 2002), but the range of values of such APG is remained to be seen. Table 1 lists the review on the effect of the APG on the riblet performance. In these papers, the pressure gradient is normalized by Clauser pressure gradient parameter

$$\beta = \frac{dp}{dx} \frac{\delta^*}{\tau_w} \quad (1)$$

or

$$\beta^+ = \frac{dp}{dx} \frac{\theta}{\tau_w}, \quad (2)$$

where  $\delta^*$ ,  $\theta$  and  $\tau_w$  represent displacement thickness, momentum thickness and wall shear stress, respectively. In Table 1, we can see that there are large variations among the reports. The minimum  $\beta$  which brings worse drag-reducing performance than zero pressure gradient (ZPG) is reported to be 0.2, whereas another paper reports that such  $\beta$  is between 3 and 3.5. The lower three papers in the table reported that the deterioration does not occur in the rage of  $\beta$  examined. Most of these reports are experimental studies on the riblet-mounted airfoil. The concern about such experiments is the difficulty of adjustment of  $\beta$ : the control of  $dp/dx$  and precise

Table 1. Review on the drag reduction by riblet under adverse pressure gradient.

Authors	$\beta$ where deterioration starts	$\beta$ where DR is worse than ZPG	$\beta_{\max}$ examined
Sundaram et al. (1996)	1.06	1.5 - 2	2
Subashchander et al. (1996)	1.5	3 - 3.5	3.5
Sundaram et al. (1999)	0.3 (swept wing)	0.4	0.4
Squire & Savill (1989)	0.05 ( $\beta^+$ )	Unknown	Unknown
Pulvin & Truong (1990)	0.1	0.2	0.2
Debisschop & Niewstadt (1996)	-	-	2.2
Choi (1990)	-	-	3.1 ( $\beta^+$ )

Table2. Domain size, number of grid points, and spatial resolution.

	Driver Part	Developing Part (smooth surface)	Developing Part (riblet surface)
$L_x \times L_y \times L_z$	$125\theta_0 \times 100\theta_0 \times 38.4\theta_0$	$400\theta_0 \times 100\theta_0 \times 38.4\theta_0$	$400\theta_0 \times 100\theta_0 \times 38.4\theta_0$
$N_x \times N_y \times N_z$	$200 \times 128 \times 128$	$512 \times 128 \times 128$	$512 \times 128 \times 1152$
$\Delta x, \Delta y, \Delta z$	0.625, 0.009~2.86, 0.3	0.78125, 0.002~2.86, 0.3	0.78125, 0.009~2.86, 0.007~0.154

measurement of  $\delta^*$ ,  $\theta$  and  $\tau_w$  on the airfoil are difficult. So far, we cannot grasp even rough estimate of the influence of APG.

In this study, DNS of the flow above the riblet considering adverse pressure gradient is conducted to investigate the influence of APG on the riblet performance. The suction and blowing are imposed at the top of the computational domain to generate APG. The rescaling/recycling method is used to simulate the spatially-developing boundary layer. The advantage of applying blowing and suction at the upper boundary is easiness of adjusting  $dp/dx$  by controlling the suction and blowing speed. In addition,  $\delta^*$ ,  $\theta$  and  $\tau_w$  can be calculated precisely. In this paper, the results of ZPG and APG are shown. At the present stage, only the results of the flow above the smooth surface are shown as APG simulation.

### OUTLINE OF COMPUTATION

The numerical simulation of the wall turbulence above the smooth surface or riblet surface is detailed in the following. Figure 1 depicts the schematic diagram of the computational domain. Spatially-developing boundary layer without upper wall is simulated to set the the blowing and suction at the upper boundary and simulate the adverse pressure gradient. The domain consists of the driver part (Fig. 1 left) and the developing part (Fig. 1 right). The Reynolds number  $Re_\theta$  based on the momentum thickness at the inlet of both driver part and developing part,  $\theta_0$ , and free-stream velocity at the inlet,  $U_{\infty,0}$ , is set to be 300. The size of the domain, the number of grid points and the spatial resolution of each part are shown in Table 2. The driver part is set up to provide inflow conditions for the developing part. Quasi-periodic boundary conditions based on the rescaling/recycling method by Lund et al. (1998) is applied in the streamwise direction to simulate an open boundary layer where the fluid is displaced from the upper boundary. The recycle station is located  $75\theta_0$  downstream of the inlet. The upper boundary condition of wall-normal velocity at the driver part and the developing part of ZPG case is based on the streamwise development of the displacement thickness (Lund et al., (1998)). The convective outflow boundary condition is employed at both parts. The periodic boundary condition is applied in the spanwise direction, and the no-slip condition is used on the walls. The velocity profile

$$V_{top} = V_{max} \times \sqrt{2} \times \left( \frac{x_c - x}{\sigma} \right) \exp \left( \varphi - \left( \frac{x_c - x}{\sigma} \right)^2 \right), \quad (3)$$

with  $V_{max} = 0.3325$ ,  $x_c = 10^5/2^9$ ,  $\sigma = 80\sqrt{2}$ ,  $\varphi = 0.95$  (Abe, 2017) is imposed at the upper boundary of the developing part of APG case. Figure 2 shows that the profile of  $V_{top}$  is blowing and suction velocities. The developing part with riblet consists of three sections; the smooth surface section ( $0 \leq x \leq 9.375\theta_0$ ), the transient section ( $9.375\theta_0 \leq x \leq 25\theta_0$ ) and riblet section ( $25\theta_0 \leq x \leq 400\theta_0$ ). The triangular riblet with the tip angle of 90 degrees (Fig. 3) is employed. A total of 36 ribs are arranged in the spanwise direction. The spacing (pitch) of the riblet groove is set at 17 wall units based on the friction velocity at the inlet, which is reported to be the optimal spacing (Bechert et al., 1997).

The governing equations are the equation of continuity and the Navier-Stokes equation of an incompressible flow on a general curvilinear coordinate system, with the collocated arrangement of the variables. The velocity-pressure coupling is by the fractional step method. The spatial derivatives are discretized by central finite differences of second-order accuracy. The Adams-Bashforth method of second-order accuracy and Crank-Nicolson method are applied for time marching of the convective and viscous terms, respectively.

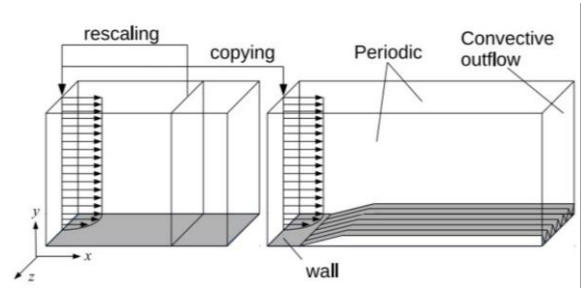


Figure 1. Computational domain.

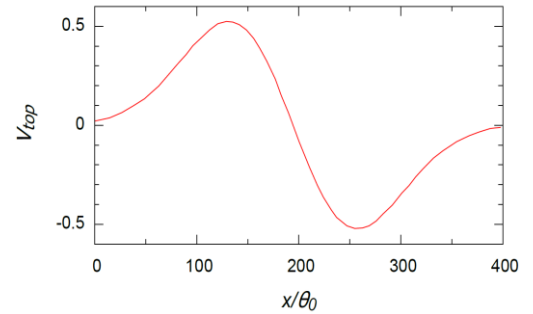


Figure 2. Blowing and suction velocities applied at the upper boundary of the developing part (Abe, 2017).

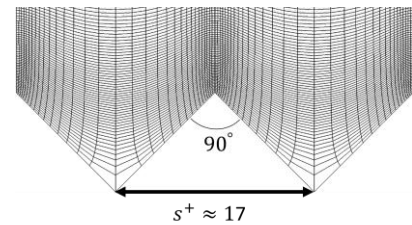


Figure 3. Computational grid near the riblet.

## RESULTS AND DISCUSSION

### Driver Part

Figure 4 represents the time series of the maximum pressure in the computational domain of the driver part. The maximum pressure increases, and a discontinuous pressure fluctuation occurs at around  $tU_{\infty,0}/\theta_0 = 1500$ . This may be because the pressure changed to satisfy the continuity equation for the increased flow rates due to an inappropriate calculation of mean velocity for rescaling simulation. As a result, at the same time, the surface-integrated wall shear stress,  $D_{smooth}$ , at the developing part also fluctuates discontinuously (described in the section of the developing part (ZPG case)). In this paper, the statistics are sampled at  $tU_{\infty,0}/\theta_0 = 400 \sim 1500$ , where the flow seems to be in quasi-steady state.

Figure 5 represents the turbulence statistics at the inlet of the driver part. The profiles are in good agreement with those calculated using spectral method (Spalart, 1988). Both RMS and Reynolds stress values are slightly larger than those of the spectral method (Spalart, 1988) at  $y^+ > 50$ . In addition, the peak value of RMS near the wall is different from those of spectral method (Spalart, 1988). These results may be caused by forming a weighted average of the profiles of the inner and outer layers in the rescaling operation (Lund et al., (1998)). This could be improved by adjusting the parameters of the weighting function, but we do not pursue further improvements in this study.

Figure 6 represents the spatial development of momentum thickness in the streamwise direction. The momentum thickness of the inlet ( $x/\theta_0 = 0$ ) is approximately unity, which is consistent with the prescribed value. Besides, the slope of  $\theta$  in the streamwise direction is about  $2.44 \times 10^{-3}$  in the present DNS. This value is approximately the same to  $2.04 \times 10^{-3}$  in the literature (Abe, 2017).

Figure 7 shows the pressure coefficient distribution at the wall surface in the streamwise direction. In this paper, pressure coefficient is defined by the following equation:

$$C_p = \frac{p - p_0}{\frac{1}{2}\rho U_{\infty,0}^2}, \quad (4)$$

where  $p_0$  is the time- and spanwise-averaged pressure at  $y = 0$  at the inlet of the driver part. The results show that the present DNS achieves the spatially-developing boundary layer under the zero pressure gradient.

The results are reasonable until the discontinuous pressure fluctuation occurs. As mentioned above, the cause of the fluctuations of pressure may be the calculation of the mean velocity which is used in the rescaling simulation.

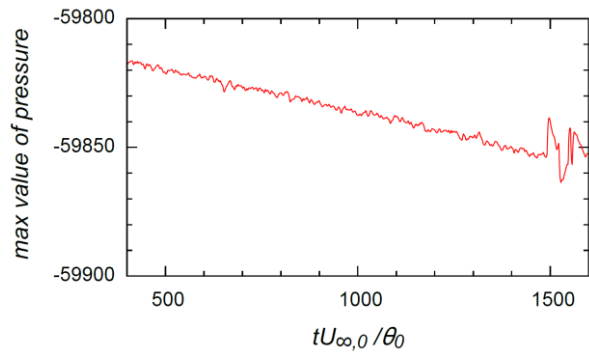
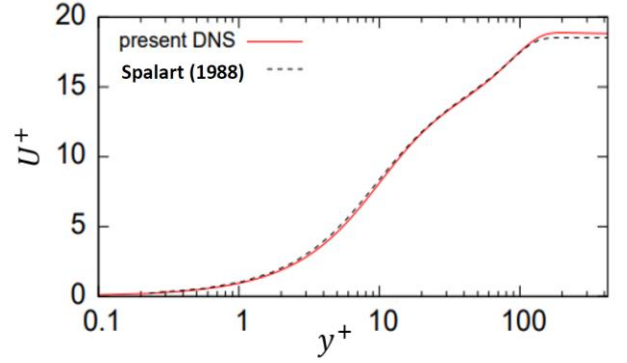
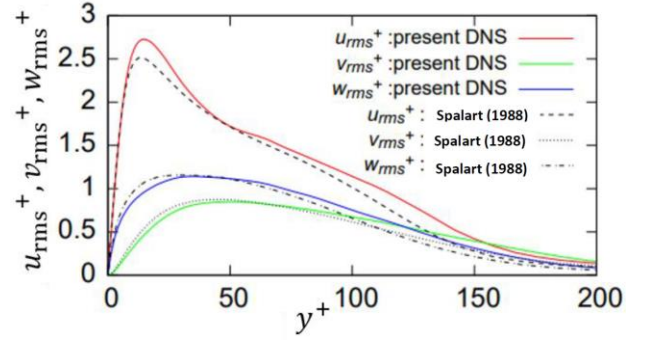


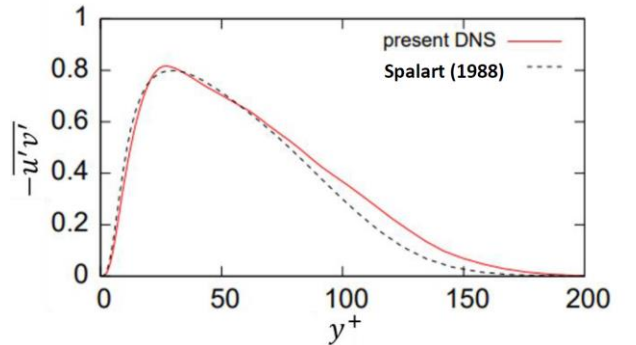
Figure 4. Time series of the maximum pressure (driver part).



(a) Mean streamwise velocity



(b) RMS fluctuation



(c) Reynolds stress

Figure 5. Turbulence statistics at the inlet of the driver part.

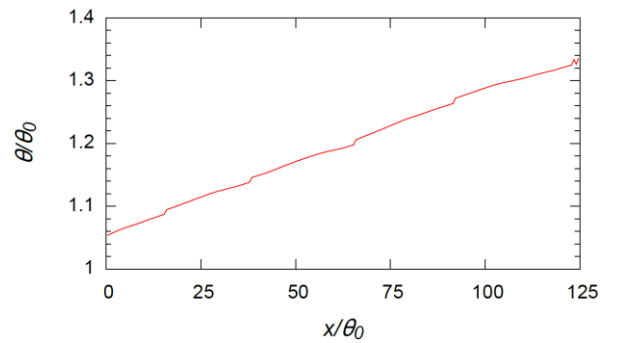


Figure 6. Spatial development of momentum thickness (driver part).

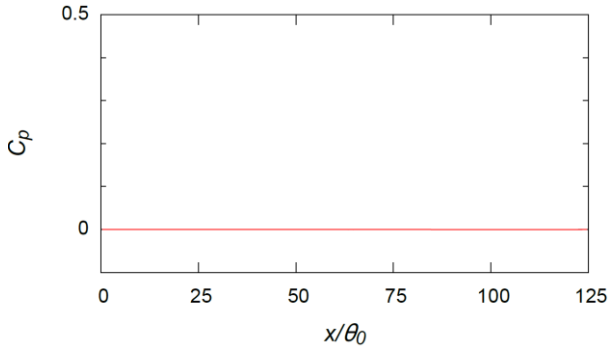


Figure 7. Pressure coefficient distribution (driver part).

### Developing Part (ZPG case)

As mentioned in the previous section, the pressure fluctuations occurring in the driver part have a harmful impact on the physical quantities in the developing part. Therefore, in this section, as in the driver part, the statistics are sampled from  $tU_{\infty,0}/\theta_0 = 400$  to 1500.

Figure 8 shows the friction coefficient distribution in the streamwise direction. The empirical model and the previous DNS results (Spalart, 1988; Abe, 2017) are also plotted for comparison. Although only in a small range ( $Re_\theta = 300 \sim 550$ ), the friction coefficient distribution of the present DNS is close to the empirical model and the results of the previous studies. Therefore, the time-averaged wall shear stress is quantitatively reproduced.

Figure 9 represents pressure coefficient distribution on the wall surface. This result shows that the present DNS achieves the spatially-developing boundary layer under the ZPG even in the developing part. We can conclude that the simulation in the developing part under the ZPG is reliable in the range of  $tU_{\infty,0}/\theta_0 = 400 \sim 1500$ . Figure 10 represents the friction drag,  $D_{smooth}$  and  $D_{rib}$ , calculated by the surface integral of the wall shear stresses on the smooth and riblet surfaces, respectively. The friction drag on the riblet surface is always smaller than that on the flat surface, which indicates the effectiveness of the riblet. The drag reduction rate calculated by the time-averaged  $D_{smooth}$  and  $D_{rib}$  equals about 3.1%, which is almost the same as the experimental value (3.4%) for a triangular straight riblet with a groove spacing of 17 wall units (Bechert et al., 1997). This implies that the DNS of the flow above the riblet surface under ZPG is also appropriately conducted.

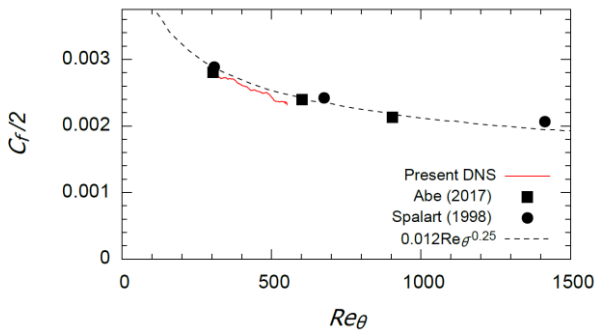


Figure 8. Friction coefficient distribution.

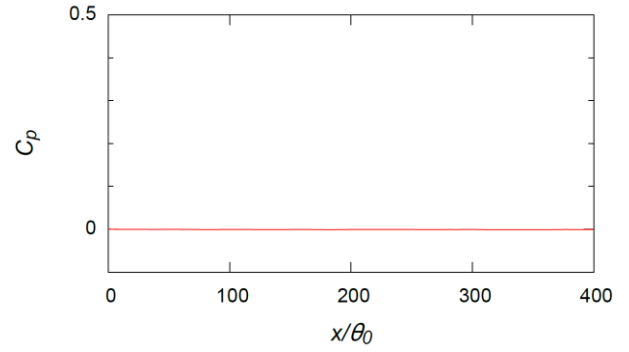


Figure 9. Pressure coefficient distribution.

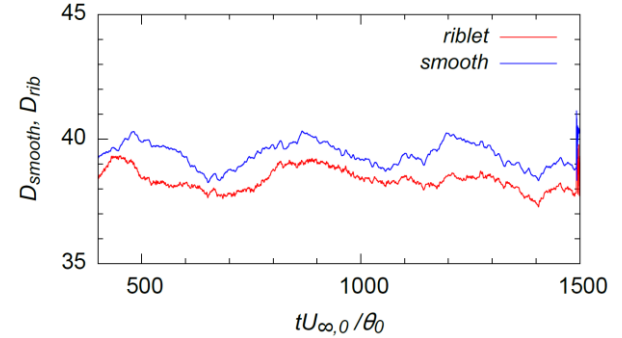


Figure 10. Comparison of the time series of the friction drag on the smooth and riblet surfaces under ZPG (developing part).

### Developing Part (APG case)

At the present stage, the results of the flow above the smooth surface under the APG are presented as a reference case of the riblet case under the APG. Figure 11 represents the friction drag,  $D_{smooth,ZPG}$  and  $D_{smooth,APG}$ , calculated by the surface integral of the wall shear stresses under the ZPG and APG, respectively. The friction drag under the APG is always smaller than that under the ZPG, which implies the existence of separation points. Figure 12 shows the friction coefficient distribution in the streamwise direction. The separation and reattachment points (i.e.  $C_f = 0$ ) are in reasonable agreement with the previous DNS result (Abe, 2017). However, the values in the present DNS are lower than those of the previous study (Abe, 2017) in other regions. This may be because the domain length of the  $y$  direction,  $L_y$ , is 25% larger than that in the previous DNS: the effect of the blowing and suction at the upper boundary reaches less on the wall in the present DNS.

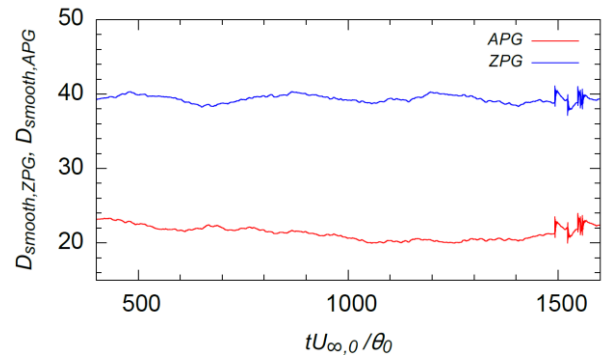


Figure 11. Comparison of the time series of the friction on the smooth surface of ZPG and APG cases (developing part).

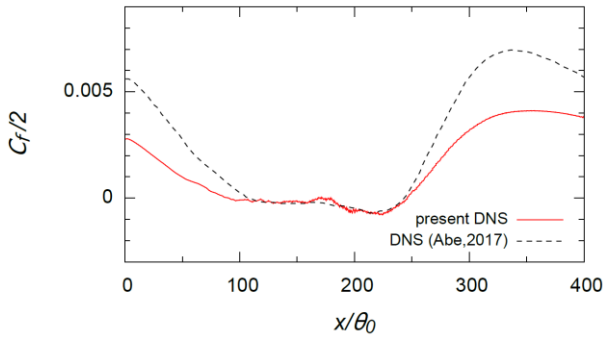


Figure 12. Friction coefficient distribution of APG case (developing part).

Figure 13 represents the pressure coefficient distribution on the wall. The maximum value of  $C_p$  is smaller than that of the previous DNS. In addition, the plateau of  $C_p$  ( $x=100\sim 200$ ) observed in the previous DNS does not appear. As mentioned above, these results are understandable considering that  $L_y$  is larger than that of the previous DNS. However, the fact that  $C_p$  does not recover to zero in the outflow indicates that the resolution is not sufficient for  $L_y$ . Grid convergence of the distributions of  $C_f$  and  $C_p$  also must be confirmed. Figure 14 shows the  $\beta$  distribution up to  $x = 60$ . The current  $\beta$  is too large compared to the values in Table 1. This implies that the strength of the suction in the present study should be weakened considering an aircraft under cruising condition.

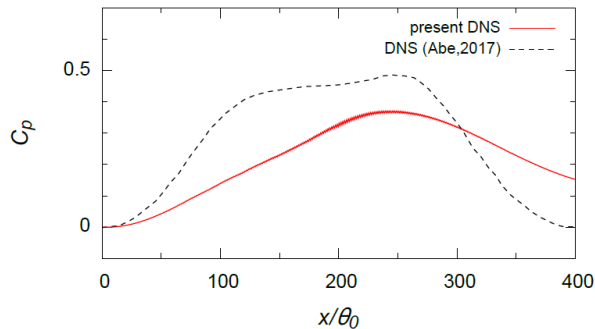


Figure 13. Pressure coefficient distribution of APG case (developing part).

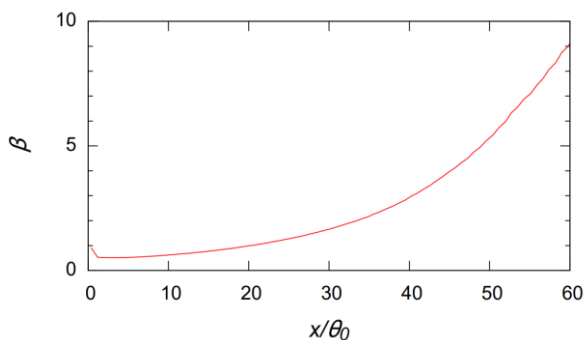


Figure 14. Clauser pressure gradient parameter  $\beta$  distribution of the region under APG (developing part).

## CONCLUSION

Direct numerical simulations (DNS) of spatially-developing wall turbulence above riblet and smooth surfaces under the zero-pressure gradient (ZPG) and adverse-pressure gradient (APG) were performed using the rescaling/recycling

method. The development of the friction coefficient, the drag-reducing performance and other statistics under the ZPG were simulated quantitatively until unphysical discontinuous pressure fluctuation occurred. The distributions of the pressure coefficient and the friction coefficient under the APG were also calculated. The separation and reattachment points are simulated qualitatively, but the results implied the lack of the resolution in the wall-normal direction.

As the next task, the calculation of the mean streamwise velocity must be revised in order to fix the unphysical pressure fluctuation in the driver part. In the developing part, grid refinement in the wall-normal direction is needed. Then, we will grasp the relationship between the value of Clauser pressure gradient parameter  $\beta$  and the strength of the blowing and suction at the upper boundary. Finally, the drag reduction effect under the APG will be investigated.

## REFERENCES

- Abe, H., 2017, "Reynolds-number Dependence of Wall-pressure Fluctuations in a Pressure-induced Turbulent Separation Bubble", *Journal of Fluid Mechanics*, Vol. 833, pp. 563-598.
- Bechert, D. W. et al., 1997, "Experiments on Drag-reducing Surfaces and their Optimization with an Adjustable Geometry", *Journal of Fluid Mechanics*, Vol. 338, pp. 59-87.
- Choi, K. S., 1990, "Effect of Longitudinal Pressure Gradient on Turbulent Drag Reduction with Riblets", in "Turbulence Control by Passive Means", Coustols, E. ed., Kluwer Academic, Dordrecht, Netherlands, pp. 109-121.
- Debisschop, J. R. and Niewstadt, F. T. M., 1996, "Turbulent Boundary Layer in an Adverse Pressure Gradient: Effectiveness of Riblets", *AIAA Journal*, Vol. 34, No. 5, pp. 932-937.
- Kurita, M. et al., 2018, "Flight Test of a Paint-riblet for reducing skin-friction", *AIAA Paper*, No. 2018-3005.
- Lund, T. S. et al., 1998, "Generation of Turbulent Inflow Data for Spatially-Developing Boundary Layer Simulations", *Journal of Computational Physics*, Vol. 140, pp. 233-258.
- Pulvin, Ph. and Truong, T. V., 1990, "Riblets in Internal Flows with Adverse Pressure Gradients", *Proceedings of the IUTAM Symposium on Structure of Turbulence and Drag Reduction*, pp.569-576.
- Spalart, P. R., 1988, "Direct Simulation of a Turbulent Boundary Layer up to  $R_\theta$  Equals 1410", *Journal of Fluid Mechanics*, Vol. 187, pp. 61-98.
- Squire, L. C. and Savill, A. M., 1989, "Drag Measurements on Planar Riblet Surfaces at High Subsonic Speeds", *Applied Science Research*, Vol. 46, pp. 229-243.
- Subashchander et al., 1996, "Drag Reduction due to Riblets on a GAW(2) Airfoil", *Journal of Aircraft*, Vol. 36, No. 5, pp. 890-892.
- Sundaram et al., 1996, "Viscous Drag Reduction Using Riblets on a NACA 0012 Airfoil to Moderate Incidence", *AIAA Journal*, Vol. 34, No. 4, pp. 676-682.
- Sundaram et al., 1999, "Viscous Drag Reduction Using Riblets on a Swept Wing", *AIAA Journal*, Vol. 37, No. 7, pp. 851-856.
- Szodruch, J., 1991, "Viscous Drag Reduction on Transport Aircraft", *AIAA Paper*, No. 91-685, pp. 1-8.
- Viswanath, P. R., 2002, "Aircraft Viscous Drag Reduction Using Riblets", *Progress in Aerospace Sciences*, Vol. 38, pp. 571-600.